Observations of He Platelets During He Ion Irradiation in 3C SiC

Benjamin T. Clay[a], Stephen E. Donnelly[a], Graeme Greaves[a]

[a]School of Computing and Engineering, University of Huddersfield, Huddersfield, HD1 3DH, UK

Keywords:

SiC
Irradiation
Fusion
Helium
In-situ TEM

Abstract

Polycrystalline 3C SiC was irradiated and observed *in-situ* via Transmission Electron Microscopy with a 20keV He ion beam at 400, 800, 1000 and 1200°C at the Microscopes and Ion Accelerators for Materials Investigations facility. During the 400, 800, 1000 and 1200°C irradiations, black-spot damage was observed at 3.1, 1.1, 2.1 and 2.1 dpa respectively. Helium bubbles were observed after 6.3 dpa at 400°C and 2.1 dpa at 800°C, and He platelets were seen after 1.1 dpa at 800, 1000 and 1200°C but not observed during the 400°C irradiation. This work shows for the first time, the preferential nucleation of platelets within stacking faults in 3C SiC. The dependence of He platelet diameter with temperature and dose has also been observed.

1. Introduction:

The proposed next generation of nuclear power stations will comprise Generation-IV [1], and fusion reactors pushing the limits of current reactor technology due to higher temperatures [2], pressures [1], and neutron fluxes [3]. Silicon carbide (SiC) is being considered for use as a plasma facing material in fusion reactors [4] and as a cladding for fission reactors due to its low activation [5], low oxidation rate [6], and high melting temperature of 2700°C [7]. 3C SiC is currently being used in Tristructural Isotropic (TRISO) fuel particles. TRISO fuel particles are small spheres (approximately 1 mm in diameter) consisting of five main components: A inner fuel kernel (typically UO_2); a porous C layer used to harbour fission products; a pyrolytic C (PyC) layer to protect the inner core from corrosion during the deposition of the 3C SiC layer; a layer of 3C SiC to withhold the high pressure gas released from the fuel; and finally another layer of PyC to protect the SiC from corrosion and to act as a backup layer to withhold the fission gasses should the SiC fail [8][9]. One advantage over conventional fuel pellets is that fission products are confined within the porous layer of the TRISO particles meaning that the fuel cladding cannot absorb the fission gasses and swell. The porous layer also makes it harder for the fission gasses to get into and poison the core. This also reduces the possibility of cracks due to differences in thermal expansion between the fuel and the cladding as the fuel particles are free to expand within the porous carbon in the TRISO particles also allowing for higher operating temperatures [10]. TRISO fuel particles are currently being used in the Japanese High Temperature Engineering Test Reactor [11][12] and in China's High Temperature Gas-Cooled Test Reactor [13]. SiC has been proposed to replace Zr cladding in Light Water Reactors (LWR) after the series of explosions at the Fukushima reactor caused by the high oxidation rate of Zr in a Loss of Coolant Accident (LOCA) [14]. This is because of the superior corrosion resistance of SiC when compared

to Zr due to a protective SiO_2 scale that forms on the SiC surface when subjected to high pressure steam at LWR LOCA related temperatures [15][16].

Decay products such as He can arise in SiC after fission reactions of the Si and C atoms due to the neutron bombardment from the fuel, and these decay products can potentially further embrittle the material in fission and fusion reactors [17]. Handbooks tabulating the He concentration via transmutations in pure Si and C, found using FISPACT-II code [18] were used to calculate the He concentration in SiC for a Pressurised Water Reactor (PWR). The FISPACT-II code calculated transmutations for each element using the average flux calculated for the fuel assembly in the P4 PWR reactor at the Paluel site in France. Silicon carbide irradiated in the average P4 flux (3.25×10^{14} n.cm^{-2}s^{-1}) for a 'full power year' will attain 10 appm He [19]. For the case of fusion, SiC in the Demonstration Reactor will obtain ≈1200 appm He due to transmutations and 150 dpa of damage after the components' lifetime of 5 years [20]. Also, plasma-wall interactions (PWIs) can occur in tokamak reactors due to plasma instabilities that can lead to plasma striking the plasma-facing materials (PFMs) and implanting high concentrations of He [21][22][23]. Because of the He build-up due to transmutations in fission/fusion reactors, and PWIs in the case of fusion, it is of great importance that the accumulation and mobility of He in SiC be understood, especially as He build-up in SiC is known to embrittle the material [24]. Studies on the formation of He platelets in SiC have been predominantly on the hexagonal polytypes, 4H and 6H [7,14,33–39,25–32]. When platelets become oversaturated with He, they have such an immense pressure (around 28 GPa) that they distort the adjacent planes in the matrix [24]. This distortion can be observed in TEM as strain fields. Fewer He platelet studies have been performed on the cubic SiC polytype, 3C [31,40,41]. Platelets in 3C SiC have been seen after annealing a sample to 1000°C that had been implanted with 65 keV He ions at 277°C to 8000 appm He [40], and also after a sample was implanted with 15.7 MeV He ions to 1000 appm He and annealed to 1050°C [31]. Platelets have also been seen in 3C SiC without annealing with simultaneous 5.1 MeV Si and 1 MeV He ion irradiation at 1000°C to approximately 600 appm He [41]. Heavier ion irradiations have not resulted in platelet formation although bubbles have still been observed. Krypton bubbles have been seen after 4 MeV Kr irradiation after annealing to 1600°C [42], and Xe bubbles have also been observed in 3C SiC crystals after 800 keV Xe ion irradiation at room temperature [43]. Although all common SiC polytypes (3C, 4H and 6H) are promising candidates for nuclear materials ([44][7][45]), 3C SiC has a greater resistance to thermal shock than 4H or 6H [6], an important property in the case of LOCAs in a fission reactor [6], and for plasma striking the PFM in a fusion reactor arising from plasma instabilities [46].

2. Experimental:

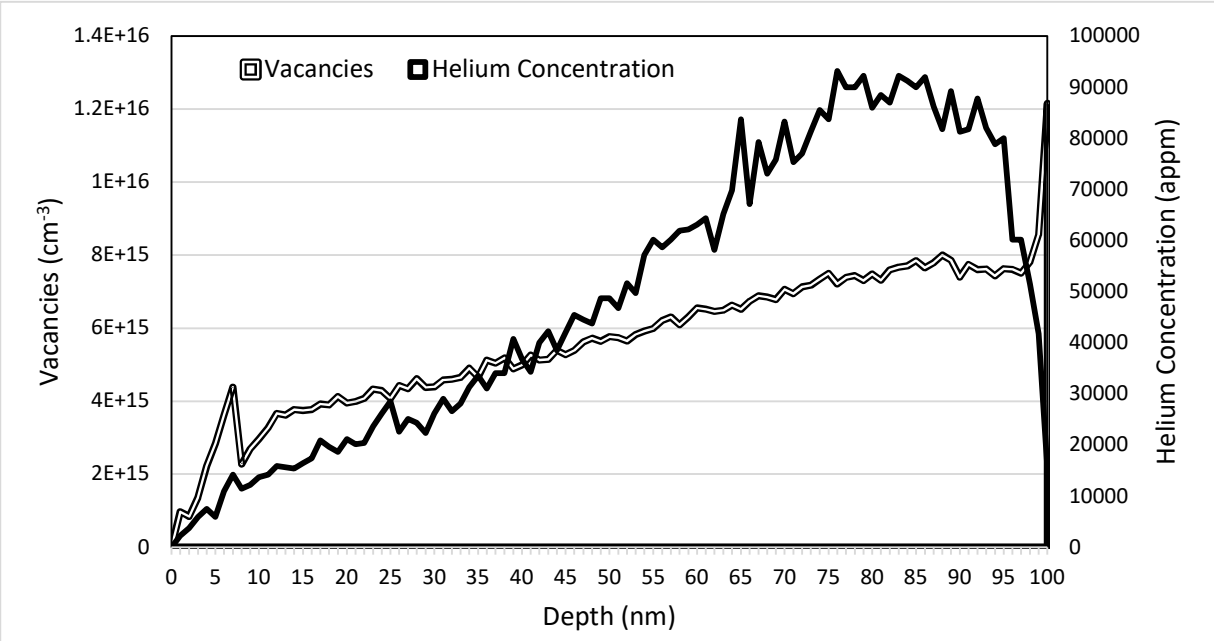

Fig 1. Plots indicating the vacancies created, and the He implanted throughout the 3C SiC samples by the 20keV He ion beam (data taken from SRIM calculations) [47].

Expected operating temperatures for PFMs in fusion reactors are in the range of 500–1100°C and so irradiation temperatures for this experiment were chosen to cover this range [2]. For the irradiations carried out at 400, 800 and 1000°C, 100 nm thick samples were created from a small block of chemical vapor deposited (CVD) polycrystalline 3C SiC with a nominal purity >99.9995% (Dow Chemical Co., high-resistivity grade). Electron transparent lamella were cut out and attached to Mo grids using the Focused Ion Beam (FIB) lift-out technique. Focused Ion Beam samples were also intended to be used at 1200°C, but upon heating these bent extensively becoming unusable. Thus, a different technique was used to produce samples for experiments at 1200°C. Thin sheets (approx. 1 mm thick) were cut from a 3C SiC block with a Well (model 3214) diamond wire saw. A Gatan (model 601) ultrasonic disc cutter was then used to cut 3 mm diameter discs out of the 3C SiC sheets, that were then thinned down to a thickness of 100 um using an Escil (model ESC 300 GTL) manual polisher. The samples were then dimpled to a thickness of around 30 µm before being finally polished in a Gatan Precision Ion Polishing System until a hole appeared in the centre of the discs. These discs maintained their structural integrity at 1200°C. Samples were then screened in either a 300 kV JEOL 3010 Transmission Electron Microscope (TEM) or a 300 kV Hitachi H-9500 TEM to ensure that they were electron transparent, and to note any crystal defects before irradiation.

The Microscopes and Ion Accelerators for Materials Investigations (MIAMI) 2 system was used for all irradiations and all *in-situ* TEM imaging [48]. MIAMI 2 features a Hitachi 9500 TEM with two ion beamlines each able to provide ions to irradiate specimens whilst under TEM examination, and the main beamline

used in this work is capable of accelerating positive singly–charged ions up to 350 keV. A Gatan 652 double-tilt heating holder was used for sample heating and imaging for the 400, 800 and 1000°C irradiations to make it easier to find low-index zones in diffraction patterns due to its double tilt capabilities. As the Gatan 652 double-tilt only has heating capabilities up to 1000°C, a Gatan 628 single-tilt heating holder was used for the heating and imaging of samples used in the 1200°C irradiations. To monitor the flux, the ion beam current was measured before and after the experiment using a Current Metering Rod located at the sample position in the TEM, and a skimming aperture located approximately 15 cm above the sample was used to monitor the current during the experiment. Due to samples being monitored *in-situ* via TEM, only thin films could be irradiated meaning that the effects of close surfaces needed to be considered.

Stopping and Range of Ions in Matter (SRIM) Monte Carlo computer code was used to calculate the displacements per atom (dpa) and the concentration of He atomic parts per million (appm) implanted into the samples [49]. A 20 keV He beam was used to give a relatively uniform damage distribution throughout the samples, as shown in figure 1. A flux of $9x10^{13}$ ions.cm^{-2}.s^{-1} was used for the 400, 800 and 1000°C irradiations, and due to a technical issue in the MIAMI 2 system, the lower $4x10^{13}$ ions.cm^{2}.s^{-1} was used for the 1200°C irradiation. All samples were irradiated to the same fluence of $2.4x10^{17}$ ions.cm^{-2} to give a peak He concentration of ≈80,000 appm (assuming that no He left the system), as this was the calculated He implanted into a PFM in the Large Helical Device [50] when using data from M. Tokitani et al [23] and SRIM (plasma flux = 10^{16} ions.cm^{-2}.s^{-1}, 2 keV He, 2 second discharge time). The samples were irradiated at 18.7° from perpendicular to the sample surface via the main beamline of MIAMI 2. The 18.7° irradiation angle and displacement energies of 20 and 35 eV for carbon and silicon respectively [51], were implemented into the SRIM calculation, and 99,999 ions with the 'Detailed Calculation with full Damage Cascade' code was used for calculating dpa. The sample thickness was also set to 100 nm and the lattice and surface energies were both set to 0 eV, and the total average damage throughout the samples in all experiments was calculated to be 8.4 dpa.

Images of the samples were taken every $3x10^{16}$ ions.cm^{-2} (1.1 dpa), and at focus, overfocus, and underfocus images were taken at each area of interest so that defects responding to phase contrast (such as bubbles) could be clearly observed. The electron beam was turned off in between imaging to minimise possible synergistic or hindering effects. Bubble diameters were measured individually using the 'line tool' in the ImageJ image manipulation software, and density was calculated by manually counting the number of bubbles in a square of known area using the same software.

3. Results:

3.1. Black Spot Damage and He Bubbles

Black spot damage became discernible in the samples after a dose of 3.1 dpa at 400°C; 1.1 dpa at 800°C, and 2.1 dpa at 1000°C. At 8.4 dpa, the highest areal density of black spots was seen in the 400 and 800°C irradiations (figure 2a and b). At 1200°C, black-spot damage was not observed but bend contours due to the undulating sample were common features (figure 2d).

Helium bubbles were only seen at 400°C after 60,000 appm (6.3 dpa) but were seen much earlier in the 800°C irradiation from 20,000 appm He (2.1 dpa). Bubbles were seen to have grown to an average (with standard deviation) of 1.6±0.28 nm in diameter after 60,000 appm (6.3 dpa) and remained at this size through the rest of the 400°C irradiation. During the 800°C irradiation, bubbles were not observed at

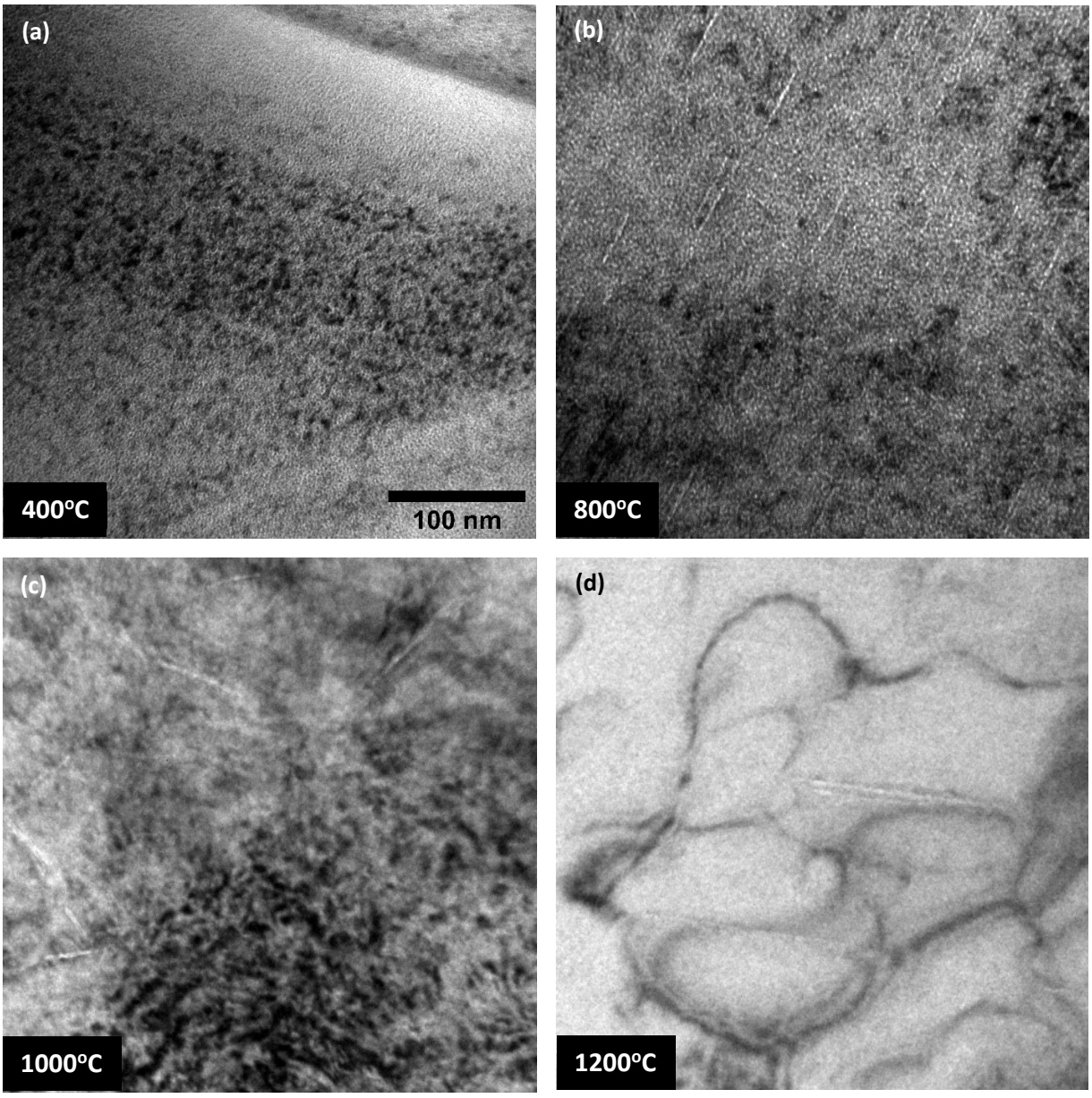

Fig 2. Bright field TEM images of 3C SiC irradiated with 20 keV He ions at dpas where prominent features were observed at each irradiation temperature (a) 400°C to 8.4 dpa at 1000 nm over-focus (Δf = +1000 nm) (b) 800°C to 8.4 dpa, Δf = -1000 nm. (c) 1000°C to 6.3 dpa, Δf = –2000 nm. (d) 1200°C to 2.1 dpa, Δf = -2000 nm. The scale marker in (a) applies to all four images.

10,000 appm (1.1 dpa) but were observed with an average diameter of 1.9±0.32 nm at 20,000 appm (2.1 dpa) and were also not observed to grow any further with higher fluence. Grain boundaries decorated with He bubbles was not a common occurrence in the 400 and 800°C irradiations, Helium bubbles were seen to decorate some grain boundaries in the 1000 and 1200°C (an example can be seen near the bottom of figure 4d) irradiations but no significant conclusions were drawn from their sizes due to the small sample size. Other bubbles were only seen within platelets in the 1000 and 1200°C irradiations (figure 3c and d).

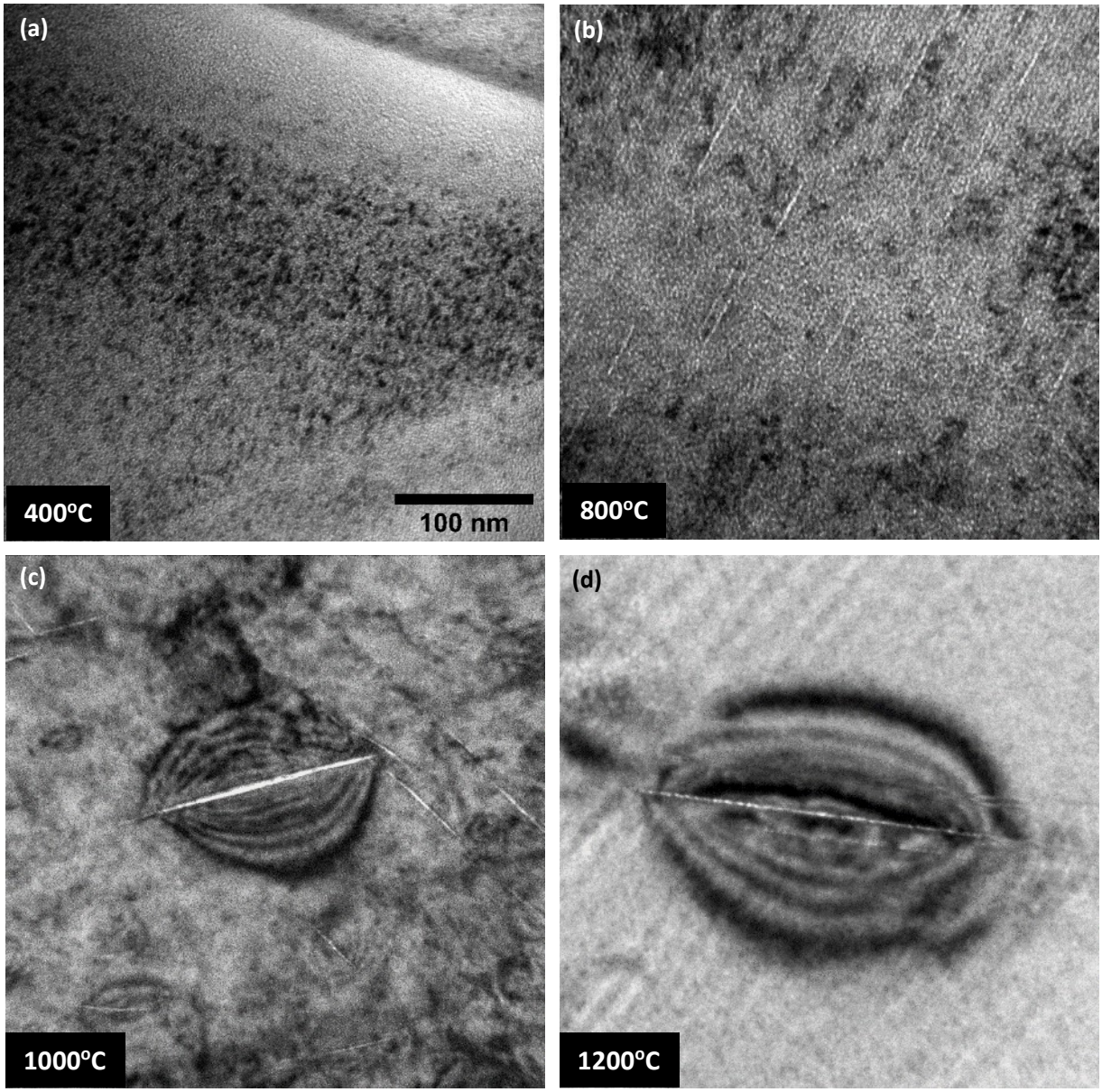

Fig 3. Bright field TEM images of 3C SiC irradiated with 20keV He ions at dpas where most prominent features were observed at each irradiation temperature. (a) 400°C, Δf = -1000 nm to 8.4 dpa. (b) 800°C to 8.4 dpa, Δf = –1000 nm. (c) 1000°C to 2.1 dpa, Δf = -2000 nm. (d) 1200°C to 1.1 dpa, Δf = –2000 nm. The scale marker in (a) applies to all four images.

3.2. Platelets

The term 'helium platelet' or 'platelet' is used in this work to describe any flat, circular defect containing He. Two types of platelet are discussed in this work: A Continuous Gas-Filled Disc (CGD) is a continuous lenticular cavity filled with He; And a bubble complex disc (BCD) is a flat, disc shaped, cluster of helium bubbles (as seen in Figures 4b and 4d). Helium platelets often exert such a high pressure on the adjacent

planes in a materials matrix (around 24 GPa [25]) that strain fields can be seen surrounding them (figures: 3c, 3d, 4a, 4c, 5a and 5b). Helium platelets show little contrast at focus (AF), appear bright in underfocus (UF), and appear dark in overfocus (OF) as they exhibit phase contrast. Smaller features exhibiting phase contrast in which they appeared light in underfocus and dark in overfocus were assumed to be He bubbles [7].

Helium platelets formed most readily at 1000°C (fig 3c) and 1200°C (fig 3d). Platelets also formed at 800°C (fig 3b) but without strain fields, and no platelets were observed at 400°C (fig 3a). Figures 6 and 7 show the variations in platelet diameters with temperature and dpa, and platelet diameters were again measured individually using the 'line tool' in the ImageJ software; The error bars shown in these graphs show the standard deviation of the platelet diameters. The platelet size increased five-fold over the temperature range studied (as shown in figure 6), but the platelets were not seen to grow larger with higher doses as illustrated in figure 7. Platelets were seen to form between the <111> and <220> planes as shown in figure 5. Throughout the 800, 1000 and 1200°C irradiations, the average platelet diameters with their standard deviations were 40±18, 60±47 and 210±75 nm respectively (with a precision of ±0.05). In the 1200°C irradiation, (022) platelets appeared to have nucleated most commonly within stacking faults as seen in figures 4a and 5b. Face-on platelets were also observed after irradiation as seen in figure 4b and 4d.

4. Discussion:

		Temperature (°C)			
Defect	**Migration Energy (eV)**	**400**	**800**	**1000**	**1200**
He interstitial	1.43[a]	717	$7x10^{6}$	$8x10^{7}$	$5x10^{8}$
C interstitial	0.88[b]	$9x10^{6}$	$3x10^{9}$	$1x10^{10}$	$4x10^{10}$
Si interstitial	1.26[b]	13400	$4x10^{7}$	$4x10^{8}$	$2x10^{9}$
C vacancy	3.5[b]	$2x10^{13}$	0.001	0.5	38
Si vacancy	3.4[b]	$1x10^{-12}$	0.004	1	86

Table 1. The migration energies and estimated jump rates of the main defects relevant to this work. The jump-rates were calculated from the Arrhenius equation and are reported in jumps.s^{-1} [52]. [a][53], [b][54].

4.1 Black Spot Damage

Black spot damage arises when highly energetic particles (such as ions) induce Primary Knock-on Atoms (PKAs) in a material. These PKAs then go on to produce collision cascades in which Frenkel pairs are formed [55]. These interstitial clusters are likely to grow in size at relatively low temperatures such as 800°C as Liu *et al.* have shown that the formation energy for interstitial clusters tends to decrease with increasing cluster size, and the 'dissociation rate of clusters is negligible as compared to the absorption rate' at 800°C [56]. At higher irradiation temperatures, black spot damage became less apparent throughout the samples. This may be due to bigger interstitial clusters breaking apart or 'dissociating' at higher temperatures as shown in table 2. It may also be due to a higher number of He atoms trapped in small vacancy clusters at lower temperatures (see section 4.2) that prevent a higher proportion of self-interstitials recombining with their vacancy counterparts, meaning that there is a greater number of self-interstitials at lower temperatures able to agglomerate into interstitial clusters. At 400°C, it can be seen (in table 2) that interstitials do not have sufficient energy to dissociate from interstitial clusters of any size

which is why in figure 2a, a high density of black-spot damage (due to interstitial clusters) can be seen. At 800°C, large black-spot defects are still observed as the interstitials do not have sufficient energy to dissociate from clusters containing 3 or more interstitials but do have sufficient energy to dissociate from di-interstitial clusters giving rise to the lower density of black-spot damage seen in figure 2b when compared to figure 2a. At 1000 and 1200°C, the interstitials have enough energy to dissociate from all interstitial clusters (up to clusters containing 6 interstitials) which explains why on average, far less black-spot damage is observed at these temperatures (figures 2c and 2d).

Dissociation Energy per Interstitial (eV) [57]	**Interstitial Cluster Size (No. of interstitials)**	**Dissociation Temperature (°C)**
2.58	2	690
3.17	3	900
3.09	4	870
3.224	5	920
3.24	6	930

Table 2. The dissociation (breaking apart) energies of carbon interstitial clusters in 3C SiC with their corresponding dissociation temperatures calculated using the Arrhenius equation. The dissociation temperature was taken as the lowest temperature that gave a dissociation rate of approximately 1 interstitial per second.

4.2 He Bubbles

At 400 and 800°C, the bubble density was not seen to increase with He fluence even though the bubbles were also not observed to grow in size. It seems unlikely that this was due the sample reaching a He saturation level and now losing most of its He at the sample's surfaces as A. Miyagawa *et al.* calculated that the He remission rate was <10% of the incoming flux at 2.4×10^{17} He ions.cm^2 (the highest fluence reached in this experiment) with a 20 keV He ion beam at 600°C [58]. Due to the difficulty of measuring the diameter of small bubbles, bubbles may have grown during these experiments up to a maximum size of 2.67 nm at 800°C, and 2.34 nm at 400°C (calculated using the error in the measurements). There was also no measurable correlation between bubble density and dose; however, a significant difference in bubble densities was measured between 400 and 800°C. The average bubble density for all doses at 400°C was measured to be 0.07±0.017 bubbles/nm^2, and for the 800°C irradiation, 0.04±0.009 bubbles/nm^2. This observation was unlikely to be due to vacancy migration as vacancies in 3C SiC are highly immobile at 800°C as the jump rates for V_c and V_{Si} were 0.001 and 0.004 j.s^{-1} respectively (as shown in table 1). Instead, it was assumed that He migrated through the samples interstitially instead of travelling in He_nV_n complexes as the main diffusion of He through SiC is believed by P. Jung to be by the "dissociation and re-trapping of trapped and clustered He atoms" (due to experimental results from 500-850°C) [59], and so the lower measured He bubble density at 800°C when compared to 400°C could be because He from smaller bubbles was able to de-trap at 800°C and migrate to the larger bubbles. If this is the case, then He is de-trapping from an abundant defect at an energy between 1.81 and 2.89 eV (calculated using the

Arrhenius equation) which may correspond to the de-trapping of He from C vacancies (2.1 eV), and Si vacancies (2.9 eV) as calculated by R.M. Van Ginhoven *et al*. [60].

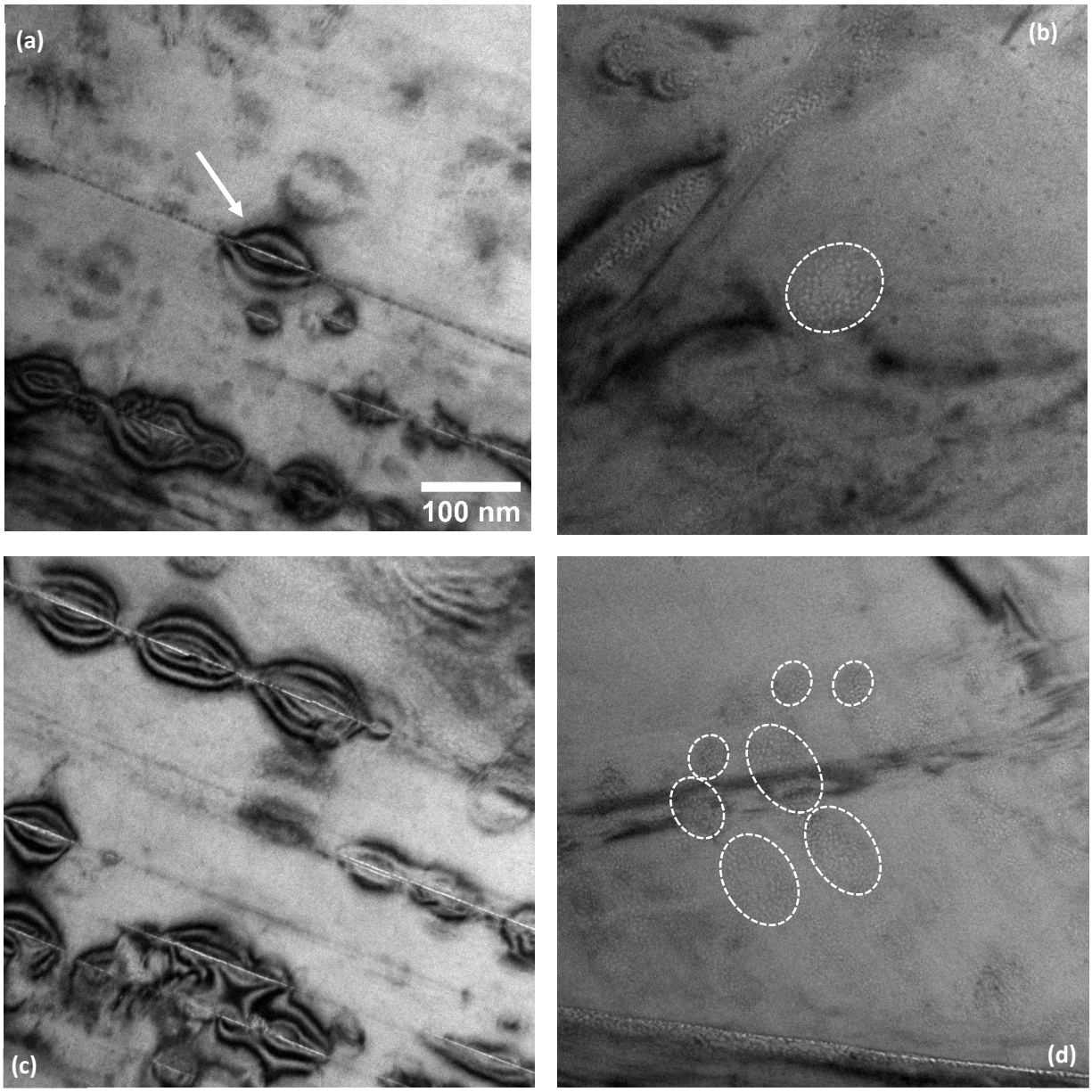

Fig 4. Bright field TEM images of 3C SiC irradiated with 20 keV He ions at 1200°C to 8.4 dpa, Δf = -1000nm. (a) Stacking fault decorated with black-spot damage and containing an edge-on He platelet (indicated by white arrow), (b) face-on platelet (indicated by white circle) with bubbles getting bigger towards the centre of the platelet, (c) edge-on platelet strings, (d) face-on platelets indicated by white circles (where platelet shape was clear). All images are of the same scale.

4.3 Helium Platelets

The absence of platelets seen during and after irradiation at 400°C is thought to be due to insufficient He interstitials in the system [7]. Although the concentration of interstitial He greatly increases at temperatures above 100°C according to desorption studies [61], there may still not be sufficient He in the system for platelets to form. At around 600°C, the same desorption study reports a further spike in interstitial He, due to the He atoms now having sufficient energy to de-trap from bigger vacancy clusters and to go on to agglomerate with again bigger vacancy clusters, as the binding energy for He_1V_4 (2.75 eV) is greater than for He_1V_1 (0.75 eV) making it energetically favourable for the He to accumulate at larger vacancy clusters [62]. This would explain why there is sufficient interstitial He for platelets to form at 800°C. The greater increase in platelet sizes between 1000 and 1200°C may have been observed due to a bigger fraction of He de-trapping from nucleation sites at 1100°C and above as documented by Miro *et al*. This temperature effect could also be seen in a similar study by Harrison *et al.* on 4H SiC where bubbles were first observed at lower temperatures of 400, 600 and 1000°C, and platelets were only observed at the highest irradiation temperature of 1200°C [7]. The observation of platelets between 800 and 1200°C was also found in 6H SiC after annealing [63]. Platelets were observed at the first irradiation step in the 800, 1000 and 1200°C irradiations meaning that platelets nucleated before 1.1 dpa and 10,000 appm He at these temperatures.

When viewed face on, platelets in this study were always observed to be of the BCD type as shown in figure 4b and d and were never observed as CGDs. Helium platelets are often reported to begin as CGDs that break down into bubble complexes/clusters (BCDs) after annealing [29][25][64]; even though this is often stated as fact, there is no visual evidence of face-on platelets that are of the CGD type. J. Chen *et al.* [25] reports observing the evolution of platelets from CGDs of He ('lenticular cavities') at 850°C, to He BCDs after annealing to +1250°C via TEM; but there are no images of face-on CGDs featured in the paper. Instead, the platelets observed edge-on at 850°C are reported to be the CGDs. It seems plausible that the edge-on platelets observed at 850°C could have been BCDs, but the individual bubbles could not be resolved as the platelets were observed edge-on, and so the 2D projection of the 3D platelet could have been made up of many overlapping bubbles that were observed as a continuous line. After annealing (to approx. 1400°C) an image in the paper [25] illustrates face-on platelets where the bubbles within the platelet were easily discernible as the projection of the platelets in the face-on orientation may have only been made up of close to one layer of bubbles [25]. The closest evidence for platelets as CGDs are those documented by M. Vallet *et al.* [65]. Although there is no mention of platelets beginning as CGDs in Vallet's paper, face-on platelets are shown to begin as bright, uniform, oval defects that could potentially be CGDs, although images again may not be at a high enough magnification to observe individual bubbles within the platelets [65]. The platelet imaged in figure 4b had the closest resemblance to a CGD in this work but again, still shows individual bubbles within its perimeter. B. Tunca *et al.* have observed the nucleation of platelets containing bubble clusters, without observing initial CGDs in a complex carbide with $(Zr_{0.5},Ti_{0.5})_2(Al_{0.5},Sn_{0.5})C$ stoichiometry, which is a double solid solution MAX phase compound. At 2 dpa and 400°C, He bubbles were seen to have nucleated within the matrix, and with further irradiation steps, lines of He bubbles began to form. At 7.5 dpa, it was observed that these bubble lines had evolved into He platelets (viewed edge-on) as individual bubbles could no longer be discerned within the bubble lines and the bubble lines featured the characteristic, thin ellipsoidal platelet shape similar to those seen in figure 3b [66].

Because of the thickness of the samples (approximately 100 nm) the edge-on platelets over 100 nm in length observed in this work cannot possibly be circular else they would have left the material matrix. Figure 4d illustrates face-on platelets that show their oval shape.

Helium platelets of the CGD type are typically believed to begin their formation when He accumulates at interstitial sites between planes in a material with the largest interplanar spacing, referred to as the close-packed planes in a crystalline material [67]. When enough He is present, the pressure becomes so great between these planes that the He pushes out neighbouring self-interstitial atoms (SIAs) from the lattice and migrates into the newly created vacancies forming a He bubble [7]. As more He interstitials migrate to the newly formed He bubble, the bubble becomes oversaturated with He and pushes out more neighbouring SIAs from the close-packed planes to accommodate the new He atoms [7]. This process of oversaturation and relaxation through the creation of more Frenkel-pairs continues until platelets of the CGD nature are formed [7]. The CGD are then thought to break down into individual bubbles creating BCDs as it is energetically favourable [29]. If platelets are instead always of the BCD nature then they must form in another way. It may be that Frenkel pair clusters with vacancy rich cores are formed in the material by primary knock-on atoms induced by ion irradiation [55]. The vacancies could accept He interstitials making a highly dense bubble region, and these bubbles may preferentially order themselves between a common plane. The constructive force exerted on the surrounding planes by all of the bubbles in the region may be the cause of the strain fields seen in TEM when viewed edge-on, giving rise to BCD platelets.

Platelets were observed to preferentially nucleate within stacking faults in the 3C SiC as shown in figures 4a, 4c and 5b. Stacking faults can act as defect sinks for He interstitials, and have been seen as preferential nucleation sites for bubbles in 3C SiC [35][33]. J. Xi *et al* used first priciple calculations to show that for a non-charged Si atom, the average migration energy within a stacking fault is 0.94 eV when compared to the bulk value of 1.26 eV [54]. This could mean that Si atoms can more readily reorder themselves to accommodate He clustering, and so He would be more likely to form platelets within the stacking faults. The preferential nucleation of platelets along stacking faults may not be the case for all SiC polytypes as Han *et al.* did not find platelets forming between stacking faults in 4H SiC at 1000^{o}C [30].

Platelets in this work were not observed to grow in diameter with increasing He dose after the material was first imaged at 10,000 appm He (1.1 dpa). It may have been that after the first irradiation step (1.1 dpa), the platelets had already grown to a saturation size. This phenomenon has been explained by M. Hartmann *et al.* as the result of platelets self-trapping within dislocation loops created as a result of the self-interstitials forced out of their sites by the over-pressurised He bubbles. This self-trapping may also be the reason that platelet strings (as seen in figure 4c) formed instead of one giant platelet as after the first platelet nucleated to its maximum size, there was still sufficient He along the stacking faults for more platelets to form. As gas pressure is likely a driving force for crack formation [58], and the pressure in platelets (in 4H SiC) is estimated to be around 24 GPa [25], it seems likely that in 3C SiC, stacking faults would be the first places for cracks to form after a continuous build-up of He due to stacking faults being the favourable site for platelets to nucleate. This suggests that in a fusion or fission reactor, 3C SiC with fewer stacking faults may be more resistant to cracking as there will be fewer sites for platelets to nucleate.

The reason for a lack of platelets at 800^{o}C in the experiment by Harrison *et al.* [7] and the observed platelets at 800^{o}C as seen in figure 3b, could be due to the difference in SiC polytype (4H in Harrison's work and 3C in this work), but it could also be due to the much lower peak density of implanted He at

≈40,000 appm He when compared with ≈80,000 appm He in this work. Also, in the same experiment by Harrison et al. Helium bubbles were observed to grow with He fluence at 800°C up to a saturation size of 1.7 nm, but bubble growth was not observed in the current experiment. This could be due to bubbles having reached a maximum size of ≈1.9 nm in the current experiment because of the higher levels of implanted He. The difference in measured bubble saturation size at 800°C between Harrison's work (1.7±0.3 nm) and this work (1.9±0.3 nm) could perhaps also be due to the difference in SiC polytype.

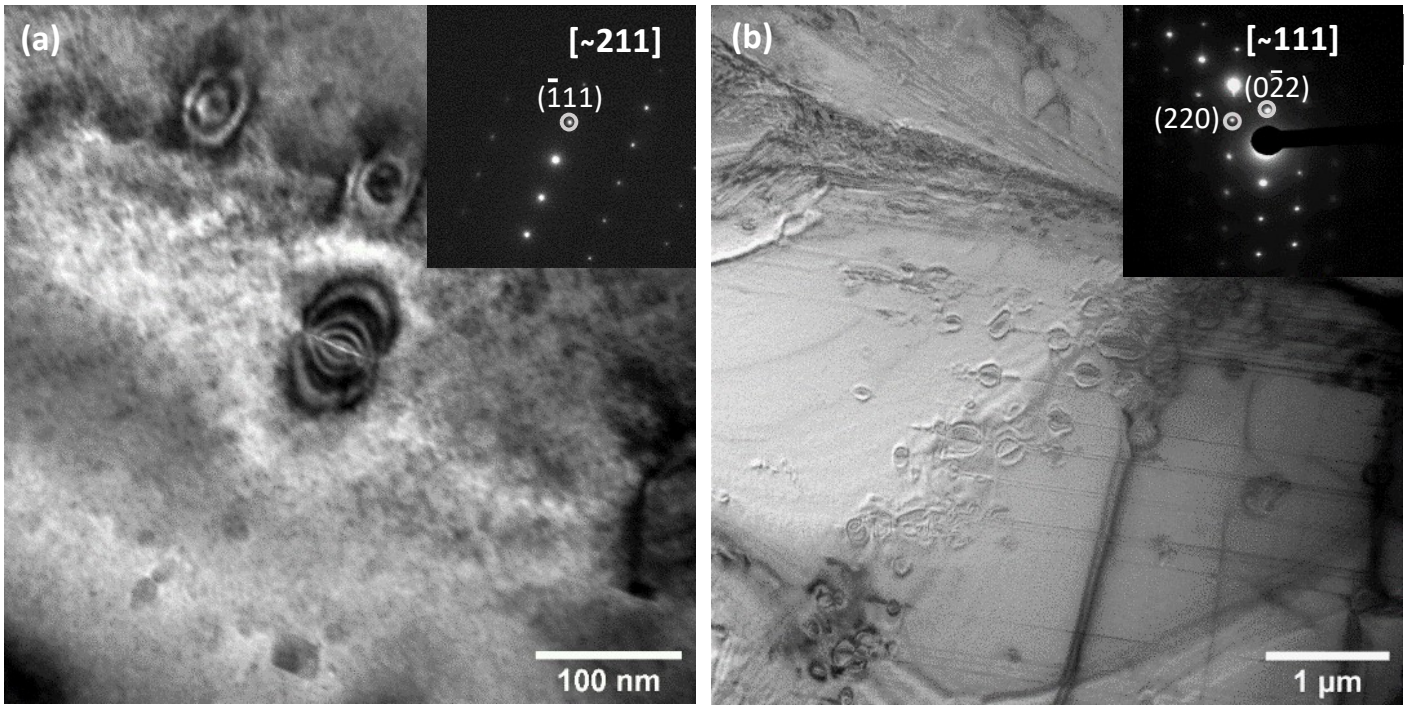

Fig 5. Bright field TEM images of 3C SiC irradiated with 20 keV He ions at (a) 1000°C to 4.2 dpa, Δf = -600 nm with inset diffraction pattern (DP) of same area. (b) 1200°C to 1.1 dpa, Δf = -2000 nm with inset DP of same area (large objective aperture).

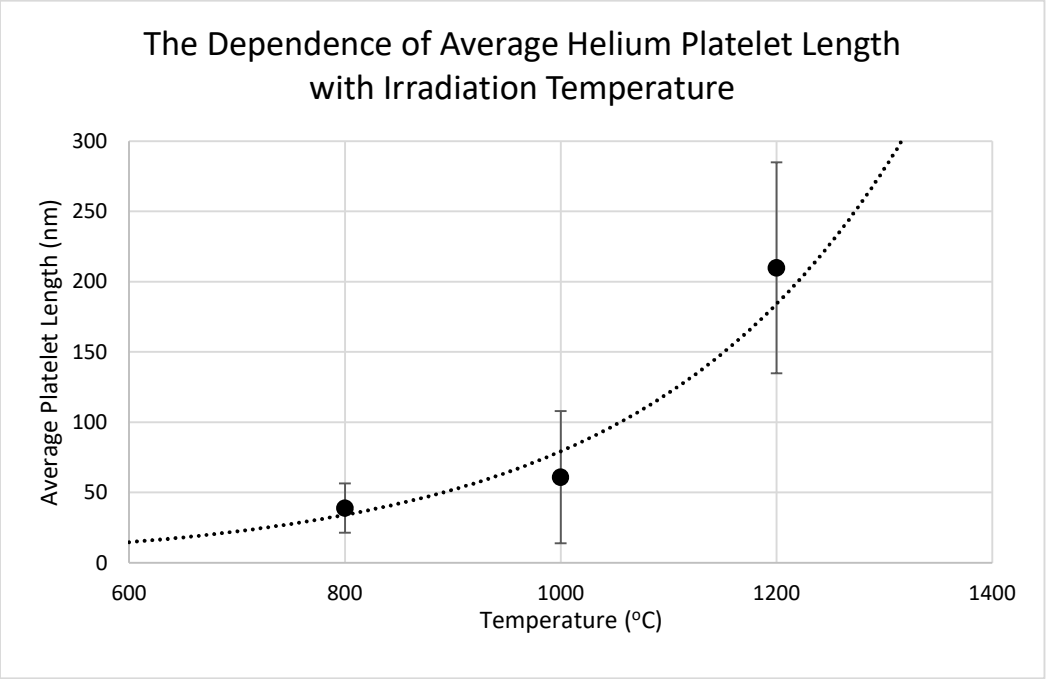

Fig 6. A graph to show the dependence of the average helium platelet length with irradiation temperature with a 20 keV He beam.

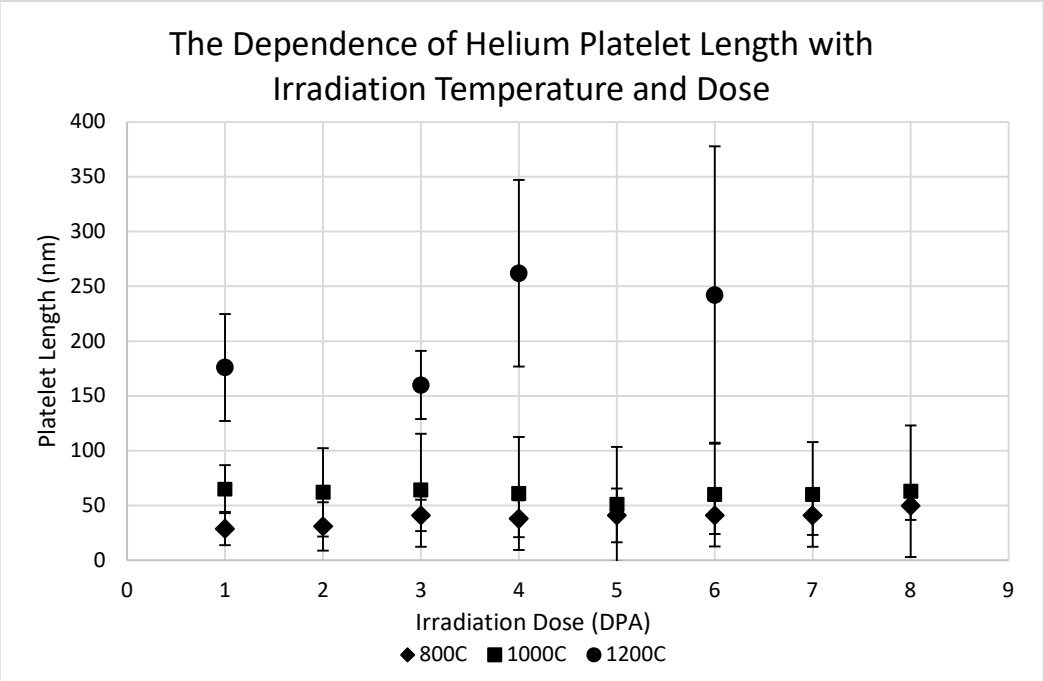

Fig 7. A graph to show the dependence of helium platelet length with irradiation temperature and irradiation dose with a 20keV He beam.

5. Conclusions:

TEM observations with *in-situ* He ion irradiation was carried out on CVD 3C SiC to observe the microstructural changes in fusion relevant conditions. Four different samples were irradiated at 400, 800, 1000 and 1200°C up to 8.4 dpa, and images were taken periodically in 1.1 dpa increments. The main conclusions drawn from this investigation are:

- Helium platelets appear to preferentially nucleate between stacking faults in polycrystalline 3C SiC under He irradiation at fusion relevant temperatures (800, 1000 and 1200°C).
- Platelets form along close-packed <111> planes and between the <220> families of planes in fusion relevant irradiation conditions.
- The higher the irradiation temperature, the greater the average platelet length that was observed.
- Platelet diameters, He bubble sizes, and bubble densities were not seen to increase with He dose.
- Detrimental defects such as cracks were not observed in the material after a high He density of 80,000 appm (similar to that expected for a SiC PFM in a fusion reactor after a PWI)
- 3C SiC grown with fewer stacking faults may nucleate less He platelets after a build-up of He, and in turn could result in a material more resistant to He embrittlement.

Acknowledgements:

The authors are grateful to P.D. Edmondson for the experimental materials provided for this work, and to EPSRC for funding the DTP studentship of the lead author, and for the funding of the MIAMI facilities (grant numbers EP/E017266/1 and EP/M028283/1).

References:

[1] T. Abram, S. Ion, Generation-IV nuclear power: A review of the state of the science, Energy Policy. 36 (2008) 4323–4330. https://doi.org/10.1016/J.ENPOL.2008.09.059.

[2] C.R.F. Azevedo, Selection of fuel cladding material for nuclear fission reactors, Eng. Fail. Anal. 18 (2011) 1943–1962. https://doi.org/10.1016/J.ENGFAILANAL.2011.06.010.

[3] M.R. Gilbert, S.L. Dudarev, D. Nguyen-Manh, S. Zheng, L.W. Packer, J.-C. Sublet, Neutron-induced dpa, transmutations, gas production, and helium embrittlement of fusion materials, J. Nucl. Mater. 442 (2013) S755–S760. https://doi.org/10.1016/J.JNUCMAT.2013.03.085.

[4] Y. Oya, Y. Onishi, T. Takeda, H. Kimura, K. Okuno, S. Tanaka, Interaction between hydrogen isotopes and damaged structures produced by He+ implantation in SiC, Fusion Eng. Des. 81 (2006) 987–992. https://doi.org/10.1016/J.FUSENGDES.2005.08.057.

[5] T. Sugiyama, Y. Morimoto, K. Iguchi, K. Okuno, M. Miyamoto, H. Iwakiri, N. Yoshida, Effects of helium irradiation on chemical behavior of energetic deuterium in SiC, J. Nucl. Mater. 307–311 (2002) 1080–1083. https://doi.org/10.1016/S0022-3115(02)01048-6.

[6] Y. Lee, Safety of light water reactor fuel with silicon carbide cladding, (2013). https://dspace.mit.edu/handle/1721.1/86866 (accessed January 31, 2018).

[7] R.. Harrison, S. Ebert, J.. Hinks, S.. Donnelly, Damage microstructure evolution of helium ion irradiated SiC under fusion relevant temperatures, Huddersfield, 2018.

[8] J.J. Powers, B.D. Wirth, A review of TRISO fuel performance models, J. Nucl. Mater. 405 (2010) 74–82. https://doi.org/10.1016/J.JNUCMAT.2010.07.030.

[9] L.L. Snead, T. Nozawa, Y. Katoh, T.-S. Byun, S. Kondo, D.A. Petti, Handbook of SiC properties for fuel performance modeling, J. Nucl. Mater. 371 (2007) 329–377. https://doi.org/10.1016/J.JNUCMAT.2007.05.016.

[10] I.D. Stoughton, N.J. Chatham, J.M. Becher, N.D. Weigel, CERAMIC COATED FUEL PARTICLES, 1964.

[11] K. Sawa, S. Ueta, Research and development on HTGR fuel in the HTTR project, Nucl. Eng. Des. 233 (2004) 163–172. https://doi.org/10.1016/J.NUCENGDES.2004.08.006.

[12] M. Ono, K. Iigaki, Y. Shimazaki, A. Shimizu, H. Inoi, D. Tochio, S. Hamamoto, T. Nishihara, S. Takada, K. Sawa, T. Kondo, K. Kojima, Confirmation of Seismic Integrity of HTTR Against 2011 Great East Japan Earthquake, in: Vol. 2 Smart Grids, Grid Stability, Offsite Emerg. Power; Adv. Next Gener. React. Fusion Technol. Safety, Secur. Cyber Secur. Codes, Stand. Conform. Assessment, Licens. Regul. Issues, ASME, 2016: p. V002T06A023. https://doi.org/10.1115/ICONE24-60571.

[13] S. Liu, Z. Li, K. Wang, Q. Cheng, D. She, Random geometry capability in RMC code for explicit analysis of polytype particle/pebble and applications to HTR-10 benchmark, Ann. Nucl. Energy. 111 (2018) 41–49. https://doi.org/10.1016/J.ANUCENE.2017.08.063.

[14] Q. Shen, G. Ran, J. Hinks, S.E. Donnelly, L. Wang, N. Li, In situ Observation of Microstructure Evolution in 4H–SiC under 3.5 keV He+ Irradiation, J. Nucl. Mater. 471 (2016) 149–153. https://doi.org/10.1016/J.JNUCMAT.2016.01.017.

[15] T. Cheng, J.R. Keiser, M.P. Brady, K.A. Terrani, B.A. Pint, Oxidation of fuel cladding candidate materials in steam environments at high temperature and pressure, J. Nucl. Mater. 427 (2012) 396–400. https://doi.org/10.1016/j.jnucmat.2012.05.007.

[16] B.A. Pint, K.A. Terrani, M.P. Brady, T. Cheng, J.R. Keiser, High temperature oxidation of fuel cladding candidate materials in steam-hydrogen environments, J. Nucl. Mater. 440 (2013) 420–427. https://doi.org/10.1016/j.jnucmat.2013.05.047.

[17] S.J. Zinkle, Advanced materials for fusion technology, Fusion Eng. Des. 74 (2005) 31–40. https://doi.org/10.1016/J.FUSENGDES.2005.08.008.

[18] J.-C.C. Sublet, J.W. Eastwood, J. Guy, M.M. Fleming, M.R. Gilbert, The FISPACT-II User Manual, 2016.

[19] M.R. Gilbert, J.-C. Sublet, Handbook of activation, transmutation, and radiation damage properties of the elements simulated using FISPACT-II & TENDL-2014; Nuclear Fission plants (PWR focus), 2015.

[20] J.C. Martinez, O. Laborde, J.J. Préjean, Material degradation under DEMO relevant neutron fluences, IOP Publishing, 2009. https://doi.org/10.1088/0031-8949.

[21] M. Rubel, Fusion Neutrons: Tritium Breeding and Impact on Wall Materials and Components of Diagnostic Systems, J. Fusion Energy. 38 (2019) 315–329. https://doi.org/10.1007/s10894-018-0182-1.

[22] M. Tokitani, H. Kasahara, S. Masuzaki, G. Motojima, M. Shoji, Y. Ueda, N. Yoshida, Y. Yoshimura, K. Nagasaki, N. Ashikawa, T. Mutoh, H. Yamada, S. Nagata, Plasma wall interaction in long-pulse helium discharge in LHD - Microscopic modification of the wall surface and its impact on particle balance and impurity generation, J. Nucl. Mater. 463 (2015) 91–98. https://doi.org/10.1016/j.jnucmat.2014.12.062.

[23] M. Tokitani, N. Yoshida, M. Miyamoto, Y. Ohtawa, K. Tokunaga, T. Fujiwara, S. Masuzaki, N. Ashikawa, M. Shoji, M. Kobayashi, A. Sagara, N. Noda, H. Yamada, A. Komori, S. Nagata, B. Tsuchiya, Evaluation of radiation damages on the first-wall surface in LHD exposed to charge-exchanged helium particles, J. Nucl. Mater. 386–388 (2009) 173–176. https://doi.org/10.1016/j.jnucmat.2008.12.086.

[24] J.H. O'Connell, J.H. Neethling, Investigation of radiation damage and hardness of H- and He-implanted SiC, Radiat. Eff. Defects Solids. 167 (2012) 299–306. https://doi.org/10.1080/10420150.2012.678008.

[25] J. Chen, P. Jung, H. Trinkaus, Microstructural evolution of helium-implanted α-SiC, Phys. Rev. B. 61 (2000) 12923–12932. https://doi.org/10.1103/PhysRevB.61.12923.

[26] S. Leclerc, M.F. Beaufort, A. Declémy, J.F. Barbot, Evolution of defects upon annealing in He-implanted 4H-SiC, Appl. Phys. Lett. 93 (2008) 122101. https://doi.org/10.1063/1.2988262.

[27] C.H. Zhang, S.E. Donnelly, V.M. Vishnyakov, J.H. Evans, Dose dependence of formation of nanoscale cavities in helium-implanted 4H-SiC, J. Appl. Phys. 94 (2003) 6017–6022. https://doi.org/10.1063/1.1611630.

[28] J. Grisolia, F. Cristiano, B. De Mauduit, G. Ben Assayag, F. Letertre, B. Aspar, L. Di Cioccio, A. Claverie, Kinetic aspects of the growth of hydrogen induced platelets in SiC, J. Appl. Phys. 87

(2000) 8415–8419. https://doi.org/10.1063/1.373556.

[29] J. Chen, P. Jung, H. Trinkaus, Evolution of Helium Platelets and Associated Dislocation Loops in α -SiC, Phys. Rev. Lett. 82 (1999) 2709–2712. https://doi.org/10.1103/PhysRevLett.82.2709.

[30] W. Han, B. Li, Microstructural defects in He-irradiated polycrystalline α-SiC at 1000 °C, J. Nucl. Mater. 504 (2018) 161–165. https://doi.org/10.1016/J.JNUCMAT.2018.03.038.

[31] P. Jung, H. Klein, J. Chen, A comparison of defects in helium implanted α- and β-SiC, J. Nucl. Mater. 283–287 (2000) 806–810. https://doi.org/10.1016/S0022-3115(00)00211-7.

[32] L. Vincent, T. Sauvage, G. Carlot, P. Garcia, G. Martin, M.F. Barthe, P. Desgardin, Thermal behaviour of helium in silicon carbide: Influence of microstructure, Vacuum. 83 (2009). https://doi.org/10.1016/j.vacuum.2009.01.017.

[33] B. Li, H. Liu, T. Shen, L. Xu, J. Wang, F. Zhao, D. Peng, J. Li, Y. Sheng, A. Xiong, Irradiation-induced microstructure damage in He-irradiated 3C-SiC at 1000℃, J. Eur. Ceram. Soc. 40 (2019) 1014–1022. https://doi.org/10.1016/j.jeurceramsoc.2019.11.026.

[34] J.F. Barbot, S. Leclerc, M.-L. David, E. Oliviero, R. Montsouka, F. Pailloux, D. Eyidi, M.-F. Denanot, M.-F. Beaufort, A. Declémy, V. Audurier, C. Tromas, Helium implantation into 4H-SiC, Phys. Status Solidi. 206 (2009) 1916–1923. https://doi.org/10.1002/PSSA.200881468.

[35] E. Aradi, J. Lewis-Fell, G. Greaves, S.E. Donnelly, J.A. Hinks, Low-temperature investigations of ion-induced amorphisation in silicon carbide nanowhiskers under helium irradiation, Appl. Surf. Sci. 501 (2020) 143969. https://doi.org/10.1016/j.apsusc.2019.143969.

[36] S. Zhao, G. Ran, Y. Guo, Q. Han, S. Liu, F. Gao, Study on the mechanism of helium platelets formation at low temperatures in SiC from the perspective of atomic diffusion, J. Nucl. Mater. 542 (2020) 152507. https://doi.org/10.1016/j.jnucmat.2020.152507.

[37] B.S. Li, C.H. Zhang, H.H. Zhang, T. Shibayama, Y.T. Yang, Study of the damage produced in 6H-SiC by He irradiation, Vacuum. 86 (2011) 452–456. https://doi.org/10.1016/J.VACUUM.2011.09.011.

[38] B. Li, V. Krsjak, J. Degmova, Z. Wang, T. Shen, H. Li, S. Sojak, V. Slugen, A. Kawasuso, Positron annihilation spectroscopy study of vacancy-type defects in He implanted polycrystalline α-SiC, J. Nucl. Mater. 535 (2020) 152180. https://doi.org/10.1016/J.JNUCMAT.2020.152180.

[39] N. Daghbouj, B.S. Li, M. Callisti, H.S. Sen, M. Karlik, T. Polcar, Microstructural evolution of helium-irradiated 6H–SiC subjected to different irradiation conditions and annealing temperatures: A multiple characterization study, Acta Mater. 181 (2019) 160–172. https://doi.org/10.1016/j.actamat.2019.09.027.

[40] C.H.H. Chen, Y. Zhang, E. Fu, Y. Wang, M.L.L. Crespillo, C. Liu, S. Shannon, W.J.J. Weber, Irradiation-induced microstructural change in helium-implanted single crystal and nano-engineered SiC, 453 (2014) 280–286. https://www.sciencedirect.com/science/article/pii/S0022311514004590 (accessed January 17, 2019).

[41] S. Kondo, T. Hinoki, A. Kohyama, Synergistic Effects of Heavy Ion and Helium Irradiation on Microstructural and Dimensional Change in β-SiC, Mater. Trans. 46 (2005) 1388–1392. https://doi.org/10.2320/matertrans.46.1388.

[42] H. Zang, W. Jiang, W. Liu, A. Devaraj, D.J. Edwards, C.H. Henager, R.J. Kurtz, T. Li, C. He, D. Yun, Z. Wang, Vacancy effects on the formation of He and Kr cavities in 3C-SiC irradiated and annealed at elevated temperatures, Nucl. Instruments Methods Phys. Res. Sect. B Beam Interact. with Mater. Atoms. 389–390 (2016) 40–47. https://doi.org/10.1016/j.nimb.2016.11.017.

[43] J. Baillet, S. Gavarini, N. Millard-Pinard, V. Garnier, C. Peaucelle, X. Jaurand, A. Duranti, C. Bernard, R. Rapegno, S. Cardinal, L. Escobar Sawa, T. De Echave, B. Lanfant, Y. Leconte, Surface damage on polycrystalline β-SiC by xenon ion irradiation at high fluence, J. Nucl. Mater. 503 (2018) 140–150. https://doi.org/10.1016/j.jnucmat.2018.01.026.

[44] S. Khalil, N. Swaminathan, D. Shrader, A.J. Heim, D.D. Morgan, I. Szlufarska, Diffusion of Ag along Σ 3 grain boundaries in 3C-SiC, Phys. Rev. B. 84 (2011) 214104. https://doi.org/10.1103/PhysRevB.84.214104.

[45] L.. Snead, J.. Hay, Neutron irradiation induced amorphization of silicon carbide, J. Nucl. Mater. 273 (1999) 213–220. https://doi.org/10.1016/S0022-3115(99)00023-9.

[46] M. Wirtz, J. Linke, G. Pintsuk, L. Singheiser, M. Zlobinski, Comparison of thermal shock damages induced by different simulation methods on tungsten, J. Nucl. Mater. 438 (2013) S833–S836. https://doi.org/10.1016/J.JNUCMAT.2013.01.180.

[47] R.E. Stoller, M.B. Toloczko, G.S. Was, A.G. Certain, S. Dwaraknath, F.A. Garner, On the use of SRIM for computing radiation damage exposure, Nucl. Instruments Methods Phys. Res. Sect. B Beam Interact. with Mater. Atoms. 310 (2013) 75–80. https://doi.org/10.1016/J.NIMB.2013.05.008.

[48] G. Greaves, A.H. Mir, R.W. Harrison, M.A. Tunes, S.E. Donnelly, J.A. Hinks, New Microscope and Ion Accelerators for Materials Investigations (MIAMI-2) system at the University of Huddersfield, Nucl. Instruments Methods Phys. Res. Sect. A Accel. Spectrometers, Detect. Assoc. Equip. 931 (2019) 37–43. https://doi.org/10.1016/J.NIMA.2019.03.074.

[49] J.F. Ziegler, The Stopping of Energetic Light Ions in Elemental Matter, 1999.

[50] A. Iiyoshi, A. Komori, A. Ejiri, M. Emoto, H. Funaba, M. Goto, K. Ida, H. Idei, S. Inagaki, S. Kado, O. Kaneko, K. Kawahata, T. Kobuchi, S. Kubo, R. Kumazawa, et al, Overview of the large helical device project, Nucl. Fusion. 39 (1999) 1245–1256. https://doi.org/10.1088/0029-5515/39/9y/313.

[51] H.L. Heinisch, L.R. Greenwood, W.J. Weber, R.E. Williford, Displacement damage cross sections for neutron-irradiated silicon carbide, J. Nucl. Mater. 307–311 (2002) 895–899. https://doi.org/10.1016/S0022-3115(02)00962-5.

[52] H. Mehrer, Diffusion in Solids, Springer Berlin Heidelberg, Berlin, Heidelberg, 2007. https://doi.org/10.1007/978-3-540-71488-0.

[53] S. Zhao, G. Ran, F. Li, H. Deng, F. Gao, Ab initio study of interstitial helium clusters in 3C-SiC, J. Nucl. Mater. 521 (2019) 13–20. https://doi.org/10.1016/J.JNUCMAT.2019.04.027.

[54] J. Xi, B. Liu, F. Yuan, Y. Zhang, W.J. Weber, Diffusion of point defects near stacking faults in 3C-SiC via first-principles calculations, Scr. Mater. 139 (2017) 1–4. https://doi.org/10.1016/J.SCRIPTAMAT.2017.06.003.

[55] K.Y. Fung, Y.R. Lin, P.J. Yu, J.J. Kai, A. Hu, Microscopic origin of black spot defect swelling in single

crystal 3C-SiC, J. Nucl. Mater. 508 (2018) 292–298. https://doi.org/10.1016/J.JNUCMAT.2018.05.054.

[56] C. Liu, L. He, Y. Zhai, B. Tyburska-Püschel, P.M. Voyles, K. Sridharan, D. Morgan, I. Szlufarska, Evolution of small defect clusters in ion-irradiated 3C-SiC: Combined cluster dynamics modeling and experimental study, Acta Mater. 125 (2017) 377–389. https://doi.org/10.1016/j.actamat.2016.12.020.

[57] C. Jiang, D. Morgan, I. Szlufarska, Structures and stabilities of small carbon interstitial clusters in cubic silicon carbide, Acta Mater. 62 (2014) 162–172. https://doi.org/10.1016/J.ACTAMAT.2013.09.044.

[58] S. Miyagawa, Y. Ato, Y. Miyagawa, Helium reemission during implantation of silicon carbide, J. Appl. Phys. 54 (1983) 2302–2306. https://doi.org/10.1063/1.332386.

[59] P. Jung, Diffusion and retention of helium in graphite and silicon carbide, J. Nucl. Mater. 191–194 (1992) 377–381. https://doi.org/10.1016/S0022-3115(09)80070-6.

[60] R.M. Van Ginhoven, A. Chartier, C. Meis, W.J. Weber, L.R. Corrales, Theoretical study of helium insertion and diffusion in 3C-SiC, J. Nucl. Mater. 348 (2006) 51–59. https://doi.org/10.1016/J.JNUCMAT.2005.09.006.

[61] E. Oliviero, M.F. Beaufort, M.F. Beaufort, J.F. Barbot, A. Van Veen, A. V Fedorov, Helium implantation defects in SiC: A thermal helium desorption spectrometry investigation, Artic. J. Appl. Phys. (2003). https://doi.org/10.1063/1.1527974.

[62] R. Li, W. Li, C. Zhang, P. Zhang, H. Fan, D. Liu, L. Vitos, J. Zhao, He–vacancy interaction and multiple He trapping in small void of silicon carbide, J. Nucl. Mater. 457 (2015) 36–41. https://doi.org/10.1016/J.JNUCMAT.2014.10.062.

[63] Q. Shen, W. Zhou, G. Ran, R. Li, Q. Feng, N. Li, Evolution of helium bubbles and discs in irradiated 6H-SiC during post-implantation annealing, Materials (Basel). 10 (2017) 101. https://doi.org/10.3390/ma10020101.

[64] T. Höchbauer, A. Misra, M. Nastasi, J.W. Mayer, Physical mechanisms behind the ion-cut in hydrogen implanted silicon, J. Appl. Phys. 92 (2002) 2335–2342. https://doi.org/10.1063/1.1494844.

[65] M. Vallet, J.-F. Barbot, S. Donnelly, J. Hinks, M.-F. Beaufort1, Hydrogen induced growth and coalescence of helium-based defects, Phys. Status Solidi. 12 (2015) 1156–1159. https://doi.org/10.1002/PSSC.201400361.

[66] B. Tunca, G. Greaves, J.A. Hinks, P.O.Å. Persson, J. Vleugels, K. Lambrinou, In situ He+ irradiation of the double solid solution (Ti0.5,Zr0.5)2(Al0.5,Sn0.5)C MAX phase: Defect evolution in the 350–800 °C temperature range, Acta Mater. 206 (2021) 116606. https://doi.org/10.1016/j.actamat.2020.116606.

[67] Y.W. You, D. Li, X.S. Kong, X. Wu, C.S. Liu, Q.F. Fang, B.C. Pan, J.L. Chen, G.N. Luo, Clustering of H and He, and their effects on vacancy evolution in tungsten in a fusion environment, Nucl. Fusion. 54 (2014) 103007. https://doi.org/10.1088/0029-5515/54/10/103007.